HOT DOT DETECTORS

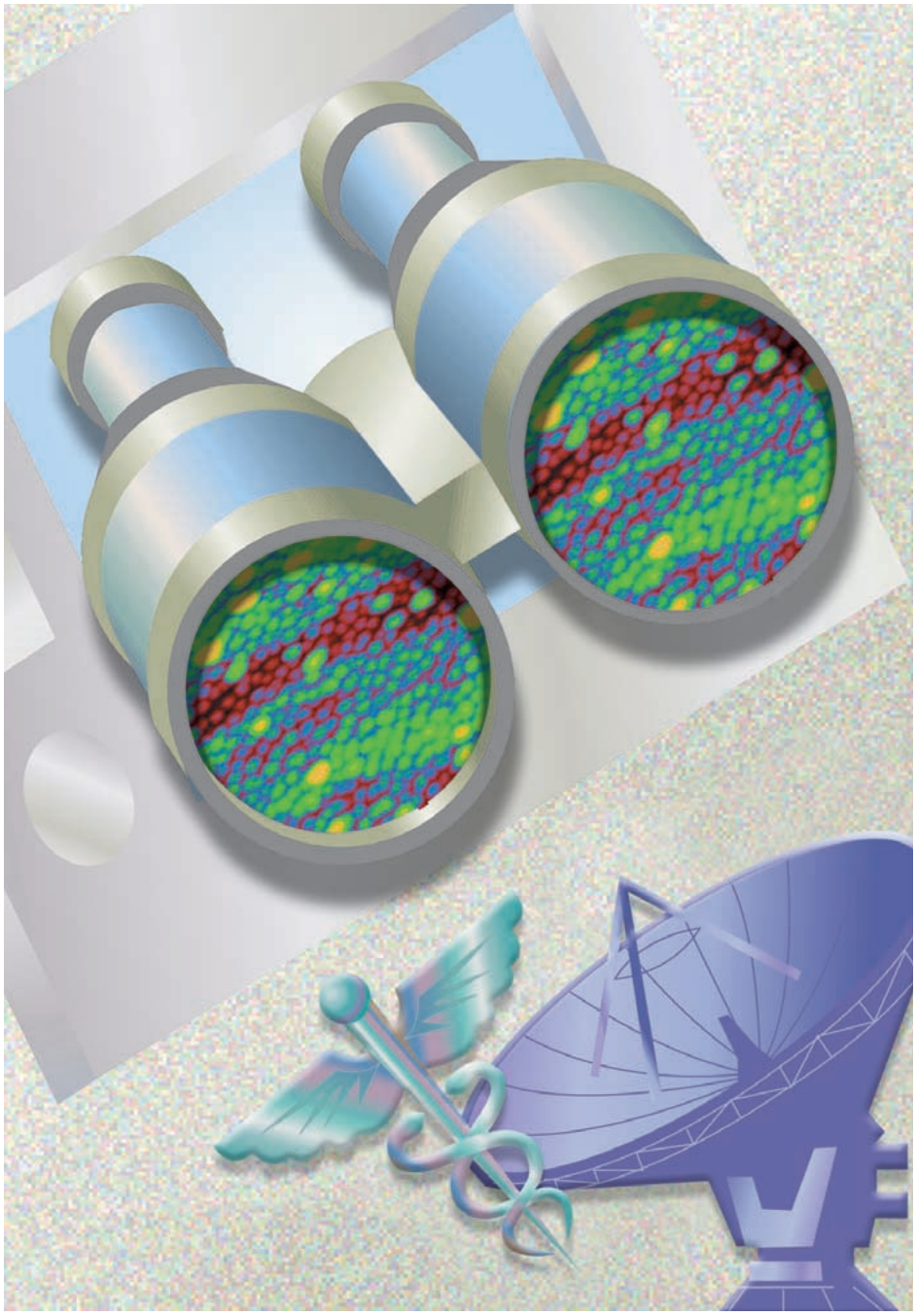

© PHOTO F/X 2

Infrared Quantum Dot Intersubband Photodetectors Are a Promising Technology for Multiwavelength IR Detection

S. Krishna,
A.D. Stiff-Roberts,
J.D. Phillips,
P. Bhattacharya, and
S.W. Kennerly

This article presents the characteristics of a relatively new device, the quantum dot infrared (IR) photodetector, or QDIP. Recent advances in the epitaxial growth of strained heterostructures, such as Ga(In)As on GaAs, have led to the realization of coherent islands through the process of self-organization. These islands behave electronically as quantum boxes, or quantum dots. The first quantum dot laser was demonstrated almost a decade ago and since then other electronic and optoelectronic devices have been reported. Theoretical and experimental studies of scattering processes and hot carrier dynamics in the quantum dots indicate that the intersubband relaxation rate of the electrons are small and may even exhibit a "phonon bottleneck," under weak excitation conditions. This property, together with the three-dimensional (3-D) carrier confinement and the near-discrete nature of the bound states,

8755-3996/02/$17.00 ©2002 IEEE

Report Documentation Page

Form Approved
OMB No. 0704-0188

1. REPORT DATE	2. REPORT TYPE	3. DATES COVERED
JAN 2002		**00-00-2002 to 00-00-2002**

4. TITLE AND SUBTITLE	5a. CONTRACT NUMBER
Hot Dot Detectors. Infrared Quantum Dot Intersubband Photodetectors Are a Promising Technology for Multiwavelength IR Detection	5b. GRANT NUMBER
	5c. PROGRAM ELEMENT NUMBER
6. AUTHOR(S)	5d. PROJECT NUMBER
	5e. TASK NUMBER
	5f. WORK UNIT NUMBER
7. PERFORMING ORGANIZATION NAME(S) AND ADDRESS(ES) **University of New Mexico,Department of Electrical and Computer Engineering,Center for High Technology Materials,Albuquerque,NM,87106**	8. PERFORMING ORGANIZATION REPORT NUMBER
9. SPONSORING/MONITORING AGENCY NAME(S) AND ADDRESS(ES)	10. SPONSOR/MONITOR'S ACRONYM(S)
	11. SPONSOR/MONITOR'S REPORT NUMBER(S)

12. DISTRIBUTION/AVAILABILITY STATEMENT
Approved for public release; distribution unlimited

13. SUPPLEMENTARY NOTES

14. ABSTRACT

15. SUBJECT TERMS

16. SECURITY CLASSIFICATION OF:			17. LIMITATION OF ABSTRACT	18. NUMBER OF PAGES	19a. NAME OF RESPONSIBLE PERSON
a. REPORT **unclassified**	b. ABSTRACT **unclassified**	c. THIS PAGE **unclassified**	**Same as Report (SAR)**	**11**	

is ideal for the design of long-wavelength intersubband detectors. Another advantage is the possibility of normal incidence operation due to the selection rules. The QDIP, therefore, has the potential of being a serious contender for applications in high-temperature IR detection, and significant progress has been made since its first demonstration nearly five years ago. The properties of these fascinating and important devices are described here. Some comparisons, in terms of dark current, are made with HgCdTe detectors and quantum-well IR photodetectors (QWIPs), two other successful technologies for IR detection.

High-performance IR systems and focal plane arrays require detectors that can demonstrate low dark current, high detectivity, high-temperature operation, and low-cost fabrication.

Overview

Infrared detectors are important for a variety of applications, including night vision, targeting and tracking, medical diagnosis, law enforcement, environmental monitoring, and space science [1]. High-performance IR systems and focal plane arrays (FPAs) require detectors that can demonstrate low dark current, high detectivity, high-temperature operation, and low-cost fabrication. At the present time, HgCdTe (MCT) interband IR detectors lead the technology. However, the narrow bandgap II-VI semiconductor material continues to pose challenges related to epitaxy and device processing, and Auger recombination severely reduces the photoexcited carrier lifetimes [1]. Quantum-well IR photodetectors are an alternative technology that uses intersubband optical transitions in quantum wells as the detection mechanism [2]. They benefit from a mature III-V growth and processing capability and have been incorporated in IR camera systems and large FPAs [3]. However, QWIPs have to operate at temperatures lower than MCT devices because of a very large rate of thermionic emission of photo-excited electrons from the quantum wells. Another disadvantage is that QWIPs cannot detect normally incident light due to polarization selection rules. This drawback is overcome by incorporating random reflectors on the top surface of the devices. Because of these shortcomings, alternative technologies are being investigated in III-V materials. One such technology is the strained layer superlattice with a type II band alignment (e.g., InAs/GaSb) [4, 5], which is expected to reduce Auger recombination rates in the detectors, thereby leading to increased operating temperatures. However, the development of these devices is still in its infancy.

A promising device that has emerged in the recent past is the quantum dot IR photodetector (QDIP) [6, 7], which, like the QWIPs, are based on optical transitions between bound states in the conduction (valence) band in quantum dots. Also, like the QWIPs, they benefit from a mature technology with large-bandgap semiconductors. Currently, self-assembled quantum dots are realized utilizing the Stranski-Krastanow growth mode of strained heterostructures, and several groups have demonstrated QDIPs with promising results [8, 9, 28, 32, 29, 30, 35, 36]. QDIPs are expected to outperform QWIPs due to a variety of reasons. First, quantum dots inherently allow sensitivity to normal excitation. The electron relaxation times between the discrete bound states, separated by 50-70 meV, are larger than in quantum wells due to a phonon bottleneck. This promises high-temperature operation of the devices. The 3-D confinement of carriers results in decreased thermionic emission and a lower dark current. Uncooled IR detectors will significantly reduce the size and operating costs of arrays and imaging systems for a variety of applications. This article aims to present intersubband quantum dot detectors as a promising technology for tunable and multiwavelength IR detection.

Self-Assembled Quantum Dots and Their Electronic Properties

Highly lattice-mismatched (mismatch ≥ 1.8%) GaInAs epitaxially grows on GaAs in the Stranski-Krastanow [10] growth mode, where self-organized islands are formed after a few monolayers of layer-by-layer growth [11-14]. For typical growth parameters used in MBE or MOVPE, an array of islands of lateral size 15-25 nm and heights 5-8 nm are formed. The coherently strained islands are, in essence, quantum dots. Elastic relaxation in the facet edges, renormalization of the surface energy of the facets, and interaction between neighboring islands via the substrate are the driving forces for self-organized growth. The optical properties and luminescence efficiencies of these dots far surpass those of quantum dots realized by selective etching of epitaxially grown quantum wells [15].

Atomic force microscopy (AFM) and transmission electron microscopy (TEM) images of InAs/GaAs quantum dots grown at the University of Michigan are shown in Fig. 1. The strain distribution in the dots has been calculated by Jiang and Singh [16], using the valence force field model [17, 18]. These authors have also determined the electronic energy levels using an eight-band kp model, which takes into account the effects of the remote bands of the bandstructure. The electronic energy levels calculated for a pyramidal $In_{0.4}Ga_{0.6}As/GaAs$ quantum dot, with base dimensions of 181 Å and height of 45 Å are shown in Fig. 2. The theoretical bandstructure calculations [16] and a variety of experimental techniques, including photoluminescence [19] and electroluminescence [20], reveal that there are a number of near-degenerate hole states and a few discrete electron states in the dots. Of these, the dominant ground and the first excited electron states are separated by 50-100 meV, depending on dot material, composition, heterostructure, and growth parameters used. The ground state is two-fold degenerate, whereas the first excited states are almost four-fold degenerate [16].

Dynamics of Hot-Carriers: Carrier Relaxation and Phonon Bottleneck

The dynamics of hot carriers in the quantum dots is very different than that in quantum wells. This became evident from the limited modulation bandwidth of interband quantum dot lasers (~5 GHz) at room temperature [21]. Theoretical studies have suggested the existence of a "phonon bottleneck" in quantum dots [22]. This prevents electron relaxation by a single phonon emission, a process that dominates carrier scattering and relaxation in quantum wells. Furthermore, since multiphonon events require the satisfaction of a stringent resonant condition, they are very slow (>1 ns). Thus, the intersubband relaxation time is expected to be much longer in quantum dots. However, recent theoretical and experimental investigations show that other scattering mechanisms such as Auger scattering [23] and electron-hole scattering [22] are responsible for carrier relaxation in quantum dots.

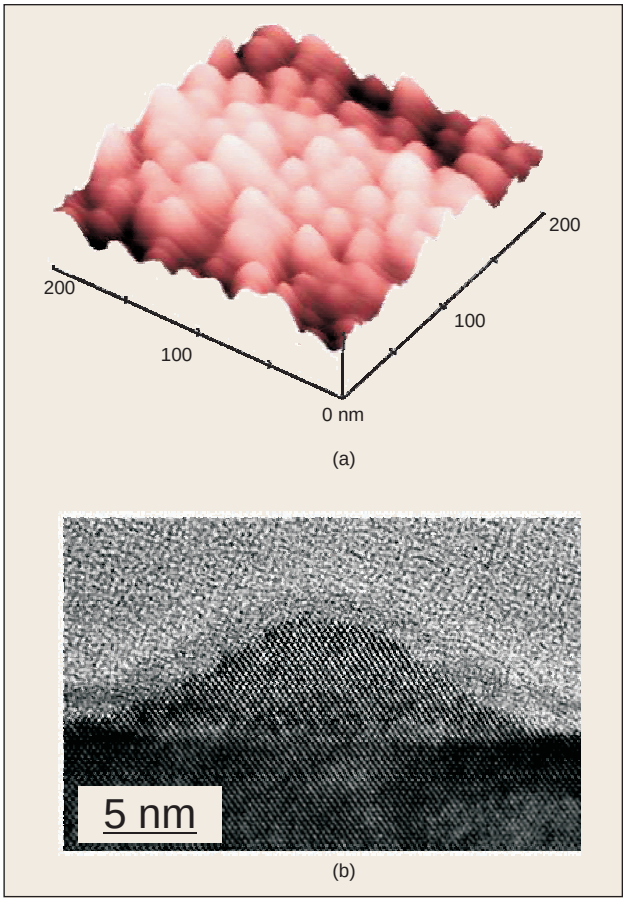

1. (a) Atomic force microscopy (AFM) and (b) transmission electron microscopy (TEM) images of self-assembled InAs/GaAs quantum dots grown by molecular beam epitaxy.

> The ultimate performance of an IR detector is commonly referred to as the background limited performance, which is the critical point where the signal becomes equal to the noise in the detector.

From a careful analysis of data obtained from both differential transmission spectroscopy (DTS) on InGaAs/GaAs quantum dot samples [24, 25] and high-frequency electrical impedance (HFEI) measurements on InGaAs/GaAs quantum dot laser diodes [26], the following picture of hot-carrier dynamics emerges. Hole relaxation times are ~0.6-0.7 ps, due to valence band mixing, anisotropy, and high density of states. Electrons relax from the barrier to the ground state in 1-2 ps. Electron relaxation from the excited state to the ground state exhibits two time constants: a short time constant (~6-8 ps), due to Auger-like processes [23], intradot electron-hole scattering [22], and multiphonon emission [27]; and a long time constant (~15-100 ps), depending on the temperature and excitation level, which is phonon-mediated and therefore demonstrates the phonon-bottleneck phenomenon. Furthermore, it is demonstrated that the faster relaxation is a geminate process, wherein the injected electron and hole are captured in the same dot, whereas the slow relaxation process is a nongeminate process, wherein the injected electrons and holes are captured in separate dots, by virtue of the sample temperature or scattering processes. It is useful to note that in quantum wells, the relaxation times are ~2-5 ps [26]. Finally, we have measured a capture time of 30-60 ps at room temperatures by analyzing the high-frequency electrical impedance response of a quantum dot laser [26]. This qualitatively agrees with the relaxation times at high temperatures as measured by DTS and as predicted by electron-hole scattering.

The long intersubband relaxation times in quantum dots can be favorably applied to intersubband detectors, which require a long-lived excited state that does not allow the rapid relaxation of photogenerated carriers. This enables their efficient contribution to the photocurrent. Moreover, the intersubband relaxation time limited by electron-hole scattering in quantum dots, unlike in QWs, increases with increase in the operating temperature, offering the possibility of realizing high-performance detectors at elevated temperatures. Together with normal incidence operation, tunability in the operating wavelength, and a broadband response (due to the size fluctuation of the self-organized quantum dots), QDIPs are poised to be serious contenders for high-temperature IR detection.

Vertical Quantum Dot Detectors

MBE Growth, Heterostructure Engineering, and Fabrication

Self-assembled InAs/Ga(Al)As quantum dot heterostructures are grown at the University of Michigan by solid-source molecular beam epitaxy (MBE) with an uncracked As_4 source on semi-insulating GaAs (100) substrates. All the detectors described here use

these multiple InAs/Ga(Al)As quantum dot layers. The vertical n-i-n structure investigated in our laboratory [28] typically has ten layers of doped InAs/Ga(Al)As quantum dots ($n = 0.5\text{-}1 \times 10^{18}$ cm^{-3}) separated by 0.025-0.1 μm of undoped GaAs spacers. AlGaAs barriers can be included in order to block dark current that results from thermionic emission, thus improving device performance. This entire absorption region is then sandwiched between highly doped GaAs contact layers to complete the n-i-n device. The general heterostructure of a typical InAs/GaAs vertical n-i-n detector is shown in Fig 3(a).

The InAs/Ga(Al)As quantum dot layers are uniformly and directly doped with silicon to provide carriers for absorption. Atomic force microscopy measurements conducted on samples with surface quantum dots grown under similar conditions indicate a dot density of 10^{10}-10^{11} dots/cm^2. Thus, the doping level corresponds to ~0.5-1 dopant atoms/dot. The doping levels in the dots and the potential barrier encountered by the carriers trapped in the dots are the two most critical parameters in the design of the vertical QDIP structure. The doping level needs to be optimized to provide 1-2 carriers per dot, so that when the device is not illuminated, the carriers are confined to the ground state of the dot and do not occupy the excited states or the continuum levels in the wetting layer. The absence of free carriers in the wetting layer ensures a lower dark current.

A simple, three-step photolithography and wet-etching process is used to fabricate the vertical QDIPs. The first step consists of Ni/Ge/Au/Ti/Au metal evaporation for the top ring contact. Next, a mesa etch (~1 μm) is performed around the top contact to define the active region for a single pixel. Finally, the metal evaporation is repeated for the bottom ring contact, which is deposited around the device mesa, and the contacts are annealed. The area of the detector exposed to IR radiation is determined by the inner radius of the top ring contact. The devices are wire bonded to a leadless chip carrier (LCC) for characterization, and a micro-photograph of wire-bonded devices mounted on a 68-pin LCC is shown in Fig. 3(b).

Spectral Response and Tuning

The spectral response of vertical InAs/Ga(Al)As QDIPs is shown in Fig. 4. As shown in Fig. 4(a), the quantum dot active region has a peak response around 4 μm when an AlGaAs barrier is present. This blue-shift occurs because higher energy carriers surmount the barrier and are collected as photocurrent. In Fig. 4(b) and (c), the peak response is approximately 8 μm and 18 μm, respectively, and no AlGaAs barrier is present in these quantum dot active regions.

Tuning by AlGaAs Barrier

It is evident that quantum dot heterostructures can be used to tune the peak response wavelength of an IR detector from 4 μm to 18 μm. The presence of an AlGaAs barrier, or lack thereof, in the heterostructure of the detector is particularly useful in tuning the peak wavelength response of the vertical QDIP. Thus, the barrier could be used not only to decrease the dark current but also to tune the position of the response peak. Therefore, two

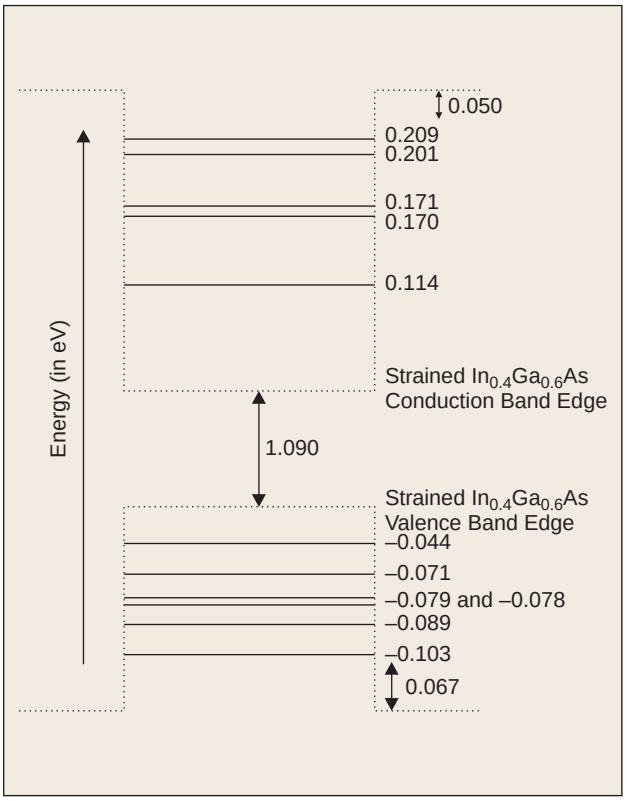

2. Calculated energy levels in a pyramidal shaped $In_{0.4}Ga_{0.6}$ As quantum dot with base dimension of 181 Å and height of 45 Å $In_{0.4}Ga_{0.6}$ As/GaAs quantum dot sample [16].

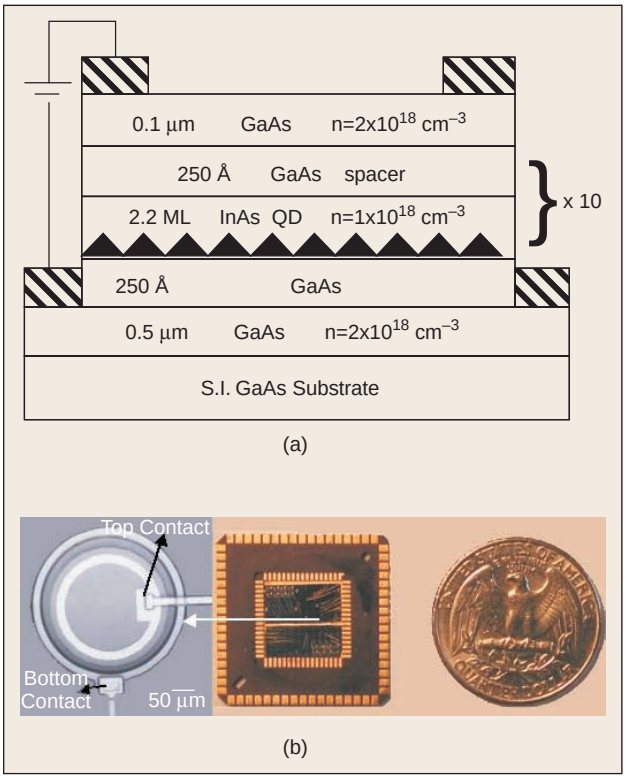

3. (a) Heterostructure of a ten-layer InAs/GaAs quantum dot IR photodetector; (b) photograph of the wire-bonded device mounted on a chip carrier.

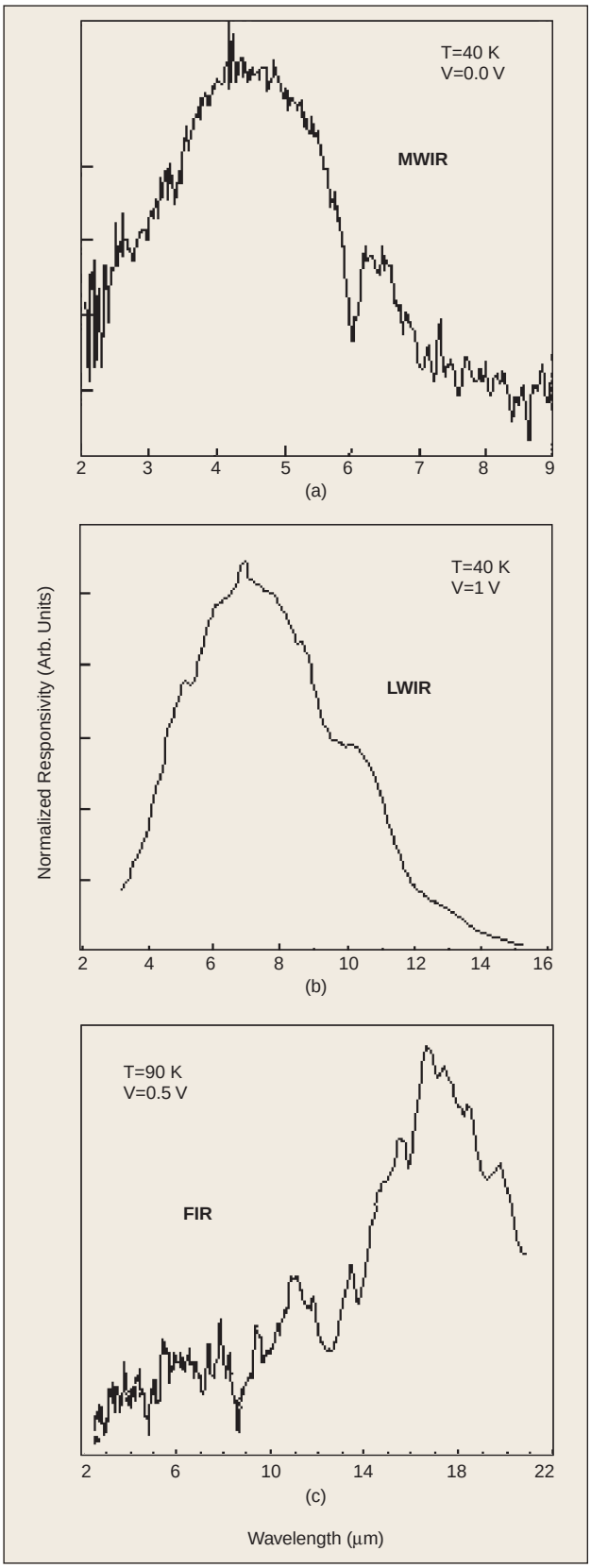

4. Spectral responses of (a) a vertical QDIP with a single 30% AlGaAs barrier in the mid-wavelength IR, and a vertical QDIP with InAs/GaAs quantum dots in the (b) long-wavelength IR and (c) far-IR wavelength ranges.

types of quantum dot heterostructures can be incorporated in the same device to realize a two-color detector [29], which is known to provide substantially more information and better resolution than a single-color detector. This is especially useful for imaging applications, where in the same epitaxial sample, quantum dot layers with the barrier could be used for mid-wavelength detection and quantum dot layers without the barrier could be used for long-wavelength detection.

Tuning by Bias Voltage

Alternatively, the spectral response of the detector could be tuned by the application of bias. This would be very convenient from a device operation point of view and will be ideal for large-area FPAs. Some of the preliminary work undertaken by us at Michigan [30] suggests that quantum dot detectors do show a change in the peak wavelength and spectral linewidth with the variation in the applied bias, as shown in Fig. 5 for a vertical QDIP with ten layers of InAs/GaAs quantum dots and a 30% AlGaAs barrier. The peak wavelength is the wavelength at which the responsivity is a maximum. The spectral linewidth, or the window of optical response (expressed as a percentage), is defined as the ratio of the full width at half maximum (FWHM) linewidth to the peak wavelength, and it is obtained from the spectral response of the detector. Note that the spectral width of these detectors is very large (~60%). This is highly desirable in many applications. It should also be noted that by changing the bias by 1 V, the peak wavelength can be tuned by almost 1 μm. We are carefully investigating this observed wavelength shift, which, if reproducible, would open up the exciting possibility of fabricating next-generation smart and adaptive FPAs *in which the external bias would determine the spectral response of each pixel.*

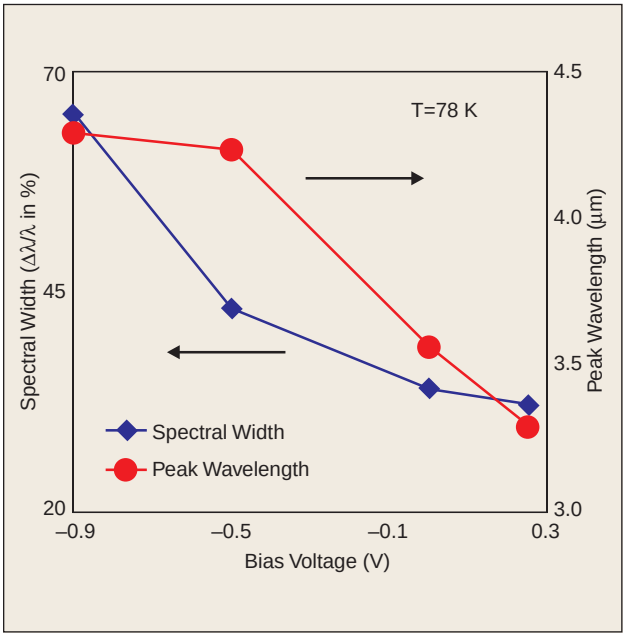

5. Measured bias-dependence of the peak wavelength λ_{peak} and the spectral width $\Delta\lambda/\lambda$ of the vertical QDIP with a single AlGaAs barrier at 78 K.

Performance Characteristics

The important parameters that characterize an IR detector at any given temperature are a) dark current, b) responsivity, c) specific detectivity (D^*), d) photoconductive gain, and e) quantum efficiency. The peak wavelength and spectral width obtained from the spectral response have already been discussed. Dark current is defined as the current flowing through the detector when there is no incident radiation, which is commonly termed the zero-field-of-view (0FOV) condition. Responsivity, measured in A/W or V/W, is defined as the ratio of the output signal to the total optical power incident on the device. Detectivity (D^*) is a measure of the signal-to-noise ratio, and it is determined by measuring the noise current i_n and then using the relation

$$D^* = R_p \sqrt{A\Delta f} \,/\, i_n \tag{1}$$

where R_p is the peak responsivity, A is the detector area, and Δf is the measurement bandwidth. The quantum efficiency is the ratio of the number of photogenerated electrons collected at the contacts to the number of incident photons. From the various vertical QDIP designs we have studied, the detectors that have demonstrated the best performance so far are ones in which a single 400 Å $Al_{0.3}Ga_{0.7}As$ barrier is incorporated alongside the active region, consisting of ten periods of 2.2 ML InAs quantum dots and 250 Å GaAs spacers. This heterostructure design, shown in Fig. 6(a), leads to a significant decrease in the dark current and an increase in the operating temperature of the detector. The measured performance characteristics of this detector are presented below.

Dark Current

The dark-current density measured at different temperatures is shown in Fig. 6(b). There is a distinct asymmetry in the dark current of the detector, and this can be explained on the basis of the asymmetry in the device heterostructure, due to the AlGaAs barrier. There is a drastic decrease in dark current in the modified quantum dot detector with AlGaAs barriers, as compared to earlier results obtained by our group. These devices also have lower dark currents than the alternative technology of QWIPs. The dark current is much lower in these QDIPs (I_d = 1.7 pA, V_b = 0.1 V, T =100 K) than in a QWIP with a similar structure and area containing three periods of 80 Å $In_{0.15}Ga_{0.85}As$ ($n = 1 \times 10^{17}$ cm^{-3})/500 Å GaAs QWs with two additional undoped 500 Å GaAs spacer layers between the quantum wells and contact layers (I_{dark}= 10 μA, V_b= 0.1 V, T = 60 K) [31].

> A bias-dependent shift in the operating wavelength has been observed in these devices, and this could be exploited to realize adaptive FPAs

Responsivity

We combined the measurement of the noise spectra and blackbody response of our QDIP for different temperatures (78 K, 100 K, 125 K, and 150 K) and varying bias voltages. An 800-K blackbody source was used to calibrate the absolute responsivity of the QDIP to normally incident IR radiation. The responsivity is determined by measuring the photocurrent induced by a calibrated blackbody source and by measuring the normalized spectral response. The photocurrent I_p is given by

$$I_p = R_p G \int_{\lambda_2}^{\lambda_1} R(\lambda) W(\lambda) d\lambda \tag{2}$$

where:

λ_i = limits over the responsivity spectrum,

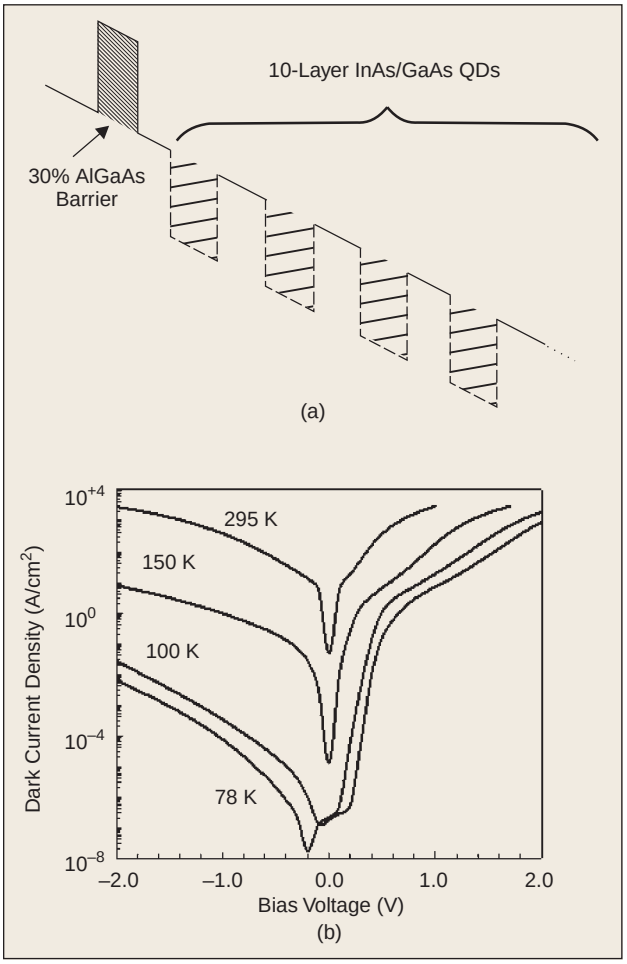

6. (a) Reverse-biased conduction band diagram of ten-layer InAs/GaAs vertical QDIP with a single 400 Å 30% AlGaAs barrier; (b) dark current density as a function of temperature for the same device.

R_p = responsivity at the peak wavelength,
$W(\lambda)$ = black-body spectral density at temperature T,
$R(\lambda)$ = normalized responsivity,
$G = \sin^2(\theta/2)AF\cos\phi$ represents all the coupling factors,
θ = optical field-of-view angle,
A = area of the detector,
F = factor that includes the transmission of the window and filters, reflectivity of detector surface, and optical beam chopper factor), and
ϕ = angle of incidence.

The normalized spectral response is obtained by using a Fourier transform IR spectrometer (FTIR). Figure 7(a) shows the measured peak responsivity for the vertical QDIP with a single AlGaAs barrier, whose heterostructure is shown in Fig. 6(a), at a temperature of 100 K. The responsivity is very low due to the presence of the AlGaAs barrier, which degrades the transport of the photogenerated carriers. Although the barrier decreases the dark current, it also decreases the photocurrent, leading to a lower responsivity.

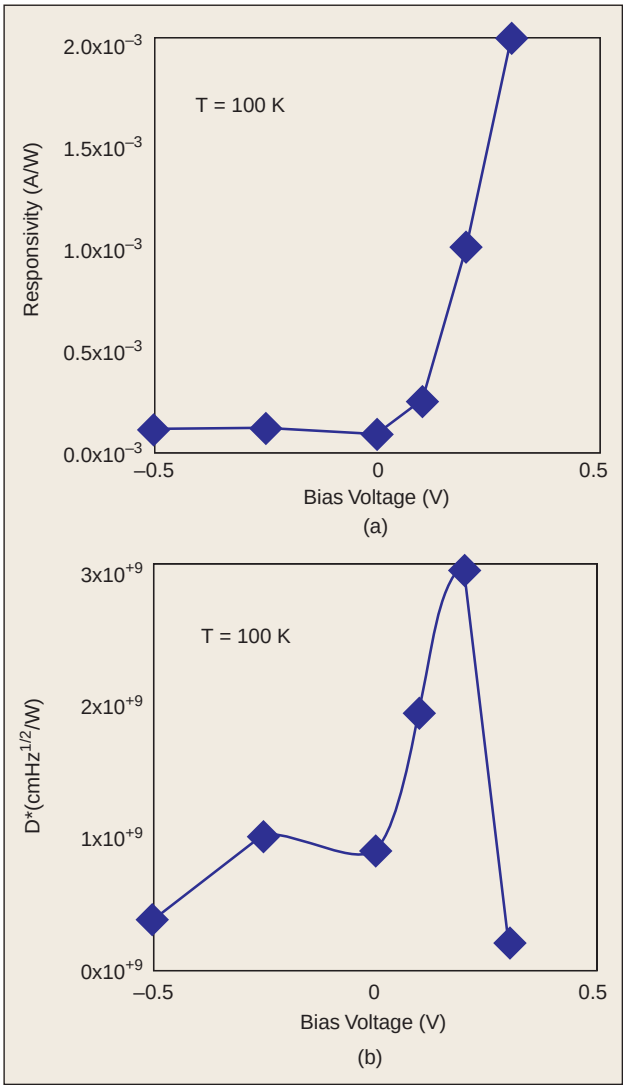

7. (a) Peak responsivity R_{peak} and (b) peak specific detectivity D as a function of bias voltage calibrated by an 800 K blackbody at a temperature of 100 K for the vertical QDIP with a single AlGaAs barrier.*

Detectivity

The detectivity is obtained from the responsivity and noise current using Eq. (1). Figure 6(b) shows the peak detectivity of the same detector as a function of bias at T = 100 K. *The measured detectivity of $D^* = 3 \times 10^9$ cmHz$^{1/2}$/W$^{1/2}$ at T = 100 K is the highest reported value of this parameter in normal-incidence, vertical quantum dot detectors.* As mentioned earlier, this same device was also characterized at a temperature as high as 150 K. *This operating temperature of 150 K is the highest reported operating temperature for any normal-incidence, vertical quantum dot detector*[32].

Photoconductive Gain

Interestingly, all the QDIPs characterized by us have exhibited photoconductive gain. It is not entirely clear what the mechanism for this gain might be, but a plausible one is as follows. Photoexcited carriers drifting across the multiple quantum dot layers can fall into a dot and kick an additional electron out, with

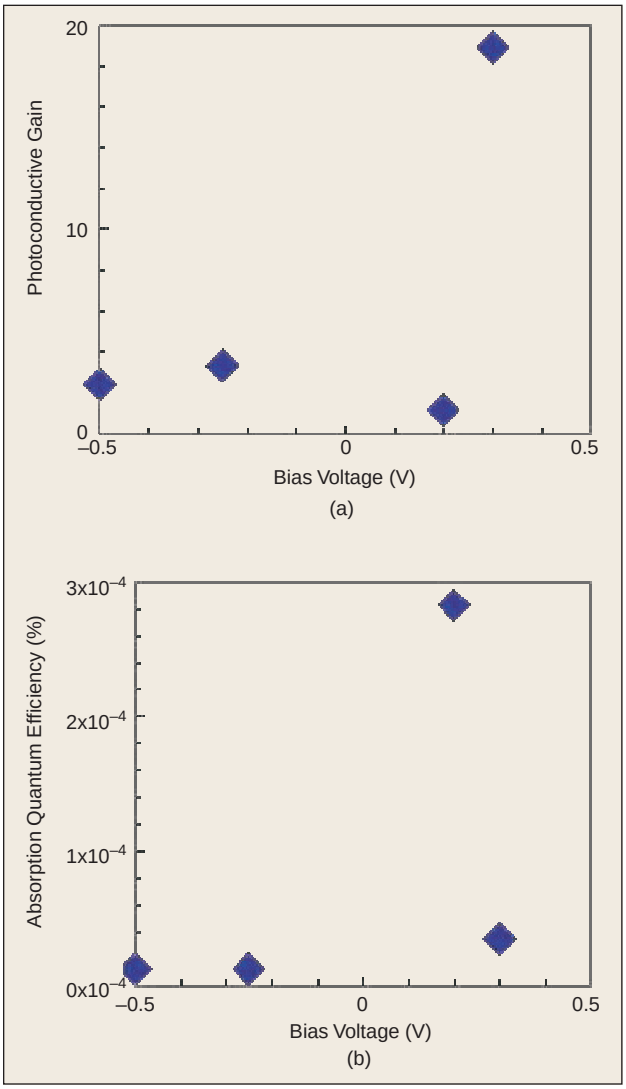

8. Measured bias-dependence of the (a) photoconductive gain and (b) absorption quantum efficiency for the vertical InAs/GaAs QDIP with a single AlGaAs barrier.

itself. This process can happen in every dot layer, leading to photocarrier multiplication and gain. A second explanation invokes the increased carrier relaxation time in the excited state of the quantum dots, which decreases the capture probability of additional free carriers.

The photoconductive gain for a QWIP can be expressed in terms of the capture probability by [33, 34]:

$$g = \frac{1}{Np(1+p)} \tag{3}$$

where p is the capture probability ($p \ll 1$) and N is the number of quantum-well layers. This equation is approximately correct for quantum dots after including an additional fill factor F in the denominator that takes into account the surface density of discrete dots across a single epitaxial layer. Since the capture probability in quantum dots is very small, the gain in QDIPs is greater than one, with expected values in the range of 1-5 [28]. The measured gain for the vertical device with a single AlGaAs barrier is shown in Fig. 8(a).

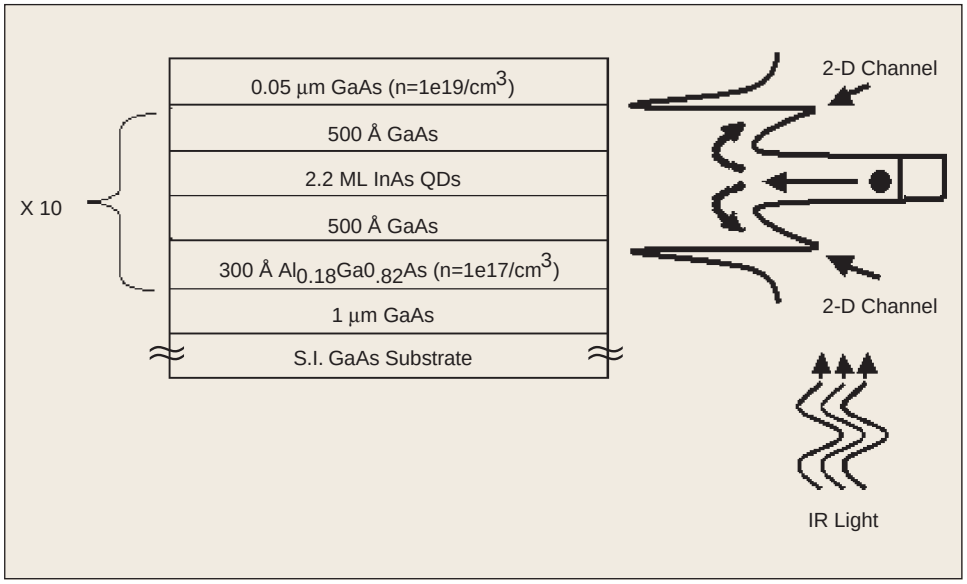

9. Heterostructure for a ten-period InAs/GaAs modulation-doped lateral QDIP with a schematic representation of the conduction band profile and photoresponse mechanism shown alongside.

Quantum Efficiency

The quantum efficiency (η_q), which can be calculated from the peak responsivity and QDIP spectral response, is defined as the ratio of collected photoexcited carriers to incident photons:

$$\eta_{\text{conv}} = \frac{hcR_{\text{peak}}}{gq\lambda_{\text{peak}}} \tag{4}$$

where λ_{peak} is the wavelength corresponding to the peak spectral response and g is the photoconductive gain. The measured quantum efficiency of the detector, whose heterostructure is shown in Fig. 6(a), is plotted in Fig. 7(b). The quantum efficiency of the quantum dot detector is very low since the carriers are better confined in the dots than in the wells. Moreover, the current-blocking AlGaAs layer decreases the number of photogenerated carriers reaching the contact. It is important to note that there is a trade-off between the spectral width and the quantum efficiency. A broad spectral response leads to decrease in quantum efficiency and vice-versa. Due to the size variation in the quantum dots, the spectral response of the detector is fairly broad, which could contribute to the decrease in the quantum efficiency.

Lateral Quantum Dot Detectors

The vertical quantum dot detectors display a large dependence of the responsivity on the doping level in the dots. Moreover, it is difficult to directly dope the dots to the desired level. To overcome this limitation, modulation-doped lateral quantum dot detectors, in which the transport of carriers occurs perpendicular to the growth direction, have been investigated [35, 36]. In this device, the dots are placed in the center of a GaAs matrix and the carriers in the dots are provided by modulation doping from the $Al_{0.18}Ga_{0.82}As$ layer, as shown in the heterostructure in Fig. 9(a).

The photoexcitation mechanism is illustrated in Fig. 9(b). Under no illumination, most of the carriers are frozen in the dots. This is corroborated by the very low dark current in these detectors, which also indicates that there is no parallel conduction through the high mobility GaAs/AlGaAs channel. The normally incident IR radiation promotes the carriers from the dots to the continuum from where they are quickly transferred to the high mobility 2-D channel on either side, due to the favorable band bending shown in Fig. 9(b). It must be noted that the spacing between the energy levels in the 2-D channel is very small, which rules out the possibility that the photoresponse arises from transitions within the 2-D modulation-doped triangular well levels.

Figure 10 summarizes the performance characteristics of the lateral detectors fabricated in our laboratory. Lee et al. [35] have demonstrated performance up to 190 K using a similar detector structure. However, the two major disadvantages of the lateral detectors are: 1) the bias voltages required for the operation of the detectors are higher than that in a vertical structure; and 2) accurate control of the number of carriers in the dots requires the inclusion of a gate making the detector a three-terminal device. Both these factors make it difficult to incorporate the lateral detectors into large-area FPAs with standard read-out circuits.

QDIP Arrays

The ultimate goal of IR detector work is to develop an IR imaging camera that consists of an FPA. This FPA, the most important component of the camera, is a hybrid, bump-bonded circuit comprised of an IR detector array to sense the IR light and a silicon read-out circuit to access each pixel of the detector array and initiate digital signal processing. The development of an entire 1024×1024 FPA, comparable in performance to those for QWIPs and MCT detectors, is an on-going project at the University of Michigan. However, such an endeavor is both expensive and time-consuming. Since we have been able to achieve promising results for single detectors, as discussed earlier, we have attempted to image a heated object with a single device, which we refer to as single-pixel imaging.

In order to conduct the measurement, we fabricated a 13×13 interconnected vertical QDIP array with a pixel diameter of 40 μm and a pitch of 120 μm. The material used in fabrication had the same heterostructure shown in Fig. 6(a). While this is not truly a single pixel, since a single average photocurrent is obtained from the entire array, the device behaves as a single pixel with a very large optical area. An X-Y pair of gold-coated mirrors servo-actuated by galvanometers is used to raster scan IR light from the object across the QDIP array. The mirror pair is mounted in a bracket whose exit window is the limiting aperture of the measurement. The QDIP array is mounted inside a cryostat with a ZnSe window in order to filter out near-IR and visible light. A lock-in amplifier is used for data acquisition. The object we chose to image is a graphite furnace igniter, which becomes red-hot when a wall current is passed through it. The image, obtained for a detector temperature of 80 K, is shown in

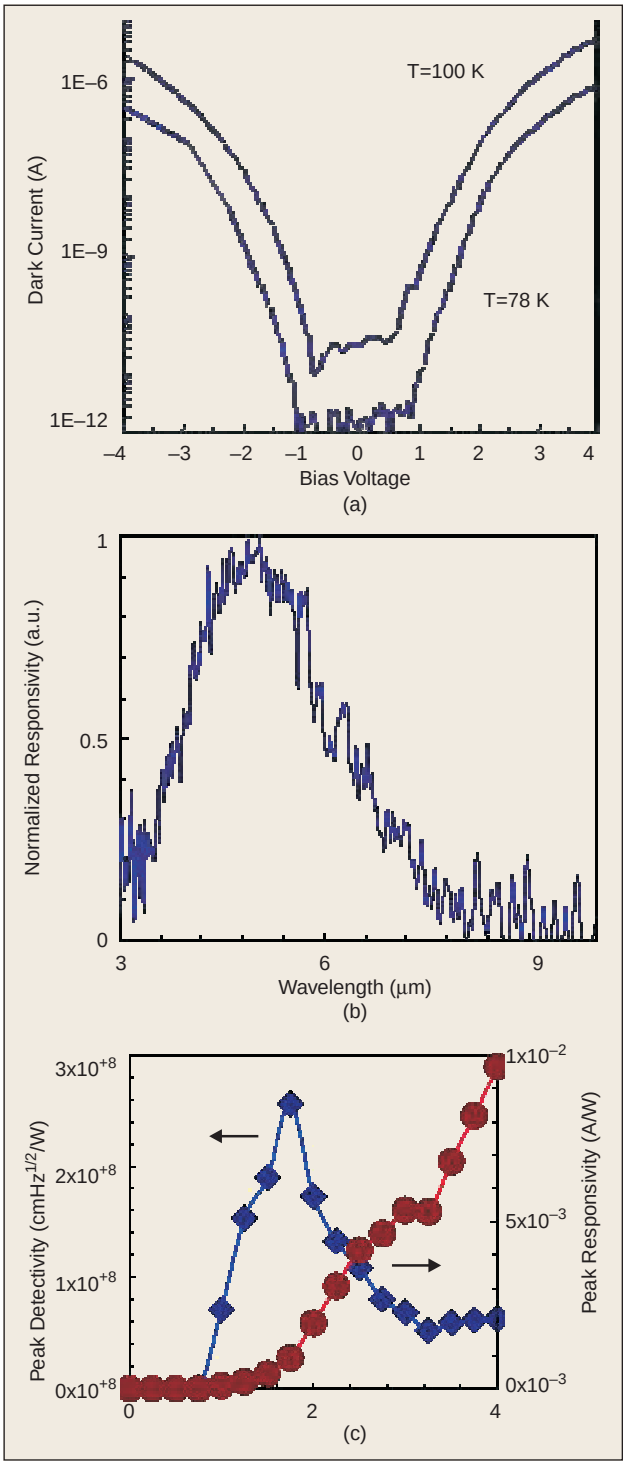

10. Performance characteristics of the 10-period InAs/GaAs modulation-doped lateral QDIP: (a) dark current, (b) spectral response, and (c) peak detectivity and responsivity.

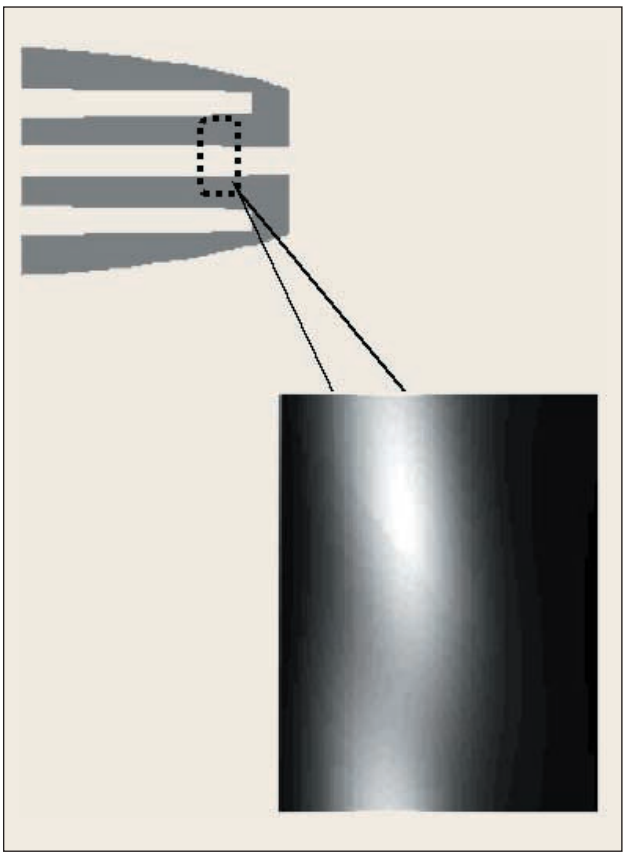

11. Raster-scanned single pixel image of a section of a graphite furnace igniter obtained at a detector temperature of 80 K for the vertical QDIP heterostructure with a single AlGaAs barrier.

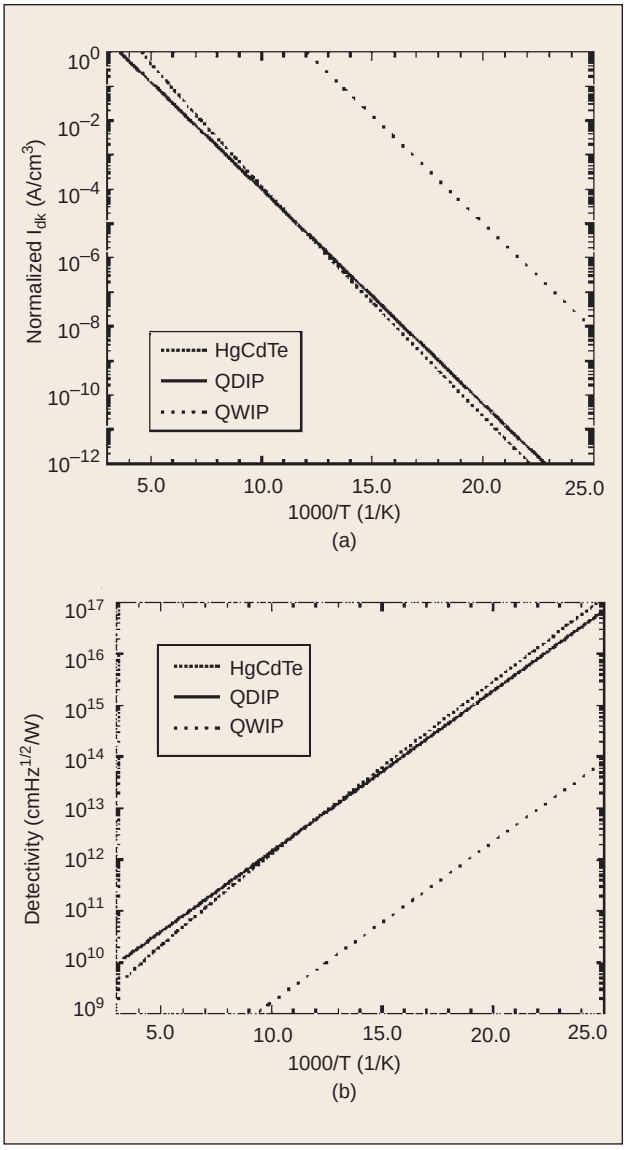

12. Comparison of thermal generation limitations on (a) normalized dark current and (b) detectivity of HgCdTe, QWIP, and QDIP detectors with a bandgap corresponding to 10 μm.

Fig. 11. A very small section of the igniter is imaged due to the limiting aperture in the X-Y mirror bracket.

Comparison of IR Detector Technologies

At this point, it is important to understand how the physics of quantum dots relate to and limit detector performance and to make comparisons with other detector materials. The ultimate performance of an IR detector is commonly referred to as the background limited performance (BLIP). This is the critical point where the signal due to the photogenerated carriers becomes equal to the noise in the detector, typically due to thermally generated carriers. Kinch has made an excellent comparison of fundamental limitations in IR detector materials through analysis of the BLIP condition [37]. This analysis allows one to evaluate a material's technology independent of device configuration and examines the BLIP condition where photogenerated carriers are greater than thermally generated carriers in the material, given by

$$\eta\Phi\tau/\tau > n_{th} \tag{5}$$

where η is the absorption quantum efficiency, Φ is the photon flux, τ is the carrier lifetime, t is the material thickness in the direction of the incident photon flux, and n_{th} is the thermally generated carrier density. Using $\eta = \alpha t$, where α is the absorption coefficient in the material, we get the BLIP requirement $\Phi > n_{th}/\alpha\tau$ and obtain a normalized thermal generation rate [37]

$$G_{th} = n_{th}/\alpha\tau. \tag{6}$$

This relationship provides a simple method of comparing fundamental differences between materials technologies for IR detectors. The dark current may then be calculated based on the thermal generation rate above. Parameters for HgCdTe and QWIPs are documented in the literature [1, 2]. For QDIPs, values of 500 ps, 5×10^4 cm^{-1}, 5×10^{10} cm^{-2}, and 1×10^{11} are used for carrier lifetime, maximum absorption coefficient, dot density, and doping density, respectively. Details of the calculation are described elsewhere [38]. A comparison for HgCdTe, QWIPs, and QDIPs is shown in Fig. 12(a) for a bandgap energy of $E_g = 0.124$ eV, corresponding to a cutoff wavelength of $\lambda_c \sim 10$ μm. In addition, a comparison of detectivity, limited by thermal generation, for HgCdTe, QWIP, and QDIP is shown in Fig. 12(b). It is clear from this analysis that because of the fundamental performance limitations, QWIPs are unlikely to rival HgCdTe devices. The performance of QDIPs, however, is predicted to rival and perhaps outperform HgCdTe detectors.

Conclusion

The properties of normal-incidence, high-temperature, mid-wavelength IR, InAs/GaAs vertical QDIPs with and without an $Al_{0.3}Ga_{0.7}As$ current-blocking barrier were discussed. These devices demonstrate very high D^* values ($D^* \sim 3 \times 10^9$ cmHz$^{1/2}$/W at $T = 100$ K and $V_{bias} = 0.2$ V) and high operating temperatures (150 K) for normal-incidence vertical QDIPs. The devices are also unique in that their high performance at low bias demonstrates their suitability for incorporation in an FPA that uses commercially available silicon read-out circuits. A bias-dependent shift in the operating wavelength has been observed in these devices, and this could be exploited to realize adaptive FPAs.

The low responsivity of these devices must be improved in order to further increase the performance of the vertical QDIP. Lateral coupling of the quantum dot ensemble may aid in this endeavor by increasing the absorption coefficient for the quantum dots. Additionally, a quantum dot superlattice with approximately 30 layers should improve the responsivity of the device.

S. Krishna (e-mail: skrishna@chtm.unm.edu), a recent graduate from the University of Michigan, is an assistant professor in the Department of Electrical Engineering and Computer Engi-

neering at the University of New Mexico in Albuquerque, New Mexico. *A.D. Stiff-Roberts* is a research assistant, *J.D. Phillips* is an assistant professor, and *P. Bhattacharya* (e-mail: pkb@eecs.umich.edu) is the James R. Mellor Professor at the University of Michigan's Department of Electrical Engineering and Computer Science in Ann Arbor, Michigan. *S.W. Kennerly* is a research scientist in the Sensors and Electron Devices Directorate of the U.S. Army Research Laboratory in Adelphi, Maryland.

References

[1] A. Rogalski, "Assessment of HgCdTe photodiodes and quantum well infrared photoconductors for long wavelength focal plane arrays," *Infrared Phys. Technol.*, vol. 40, p. 279, 1999.

[2] J.L. Pan and C.G. Fonstad, "Theory, fabrication, and characterization of quantum well infrared photodetectors," *Mat. Sci. Eng.*, vol. 28, p. 65, 2000.

[3] S.D. Gunapala, S.V. Bandara, A. Singh, J.K. Liu, B. Rafol, E.M. Luong, J.M. Mumolo, N.Q. Tran, D.Z.Y. Ting, J.D. Vincent, C.A. Shott, J. Long, and P.D. LeVan, "640 x 486 long-wavelength two-color GaAs/AlGaAs quantum well infrared photodetector (QWIP) focal plane array camera," *IEEE Trans. Electron. Devices*, vol. 47, p. 963, May 2000.

[4] C. Mailhiot and D.L. Smith, "Long-wavelength infrared detectors based on strained InAs-Ga1-xInxSb type-II superlattices," *J. Vac. Sci. Technol. A*, vol. 7, p. 445, 1989.

[5] F. Fuchs, U. Weimer, W. Pletschen, J. Schmitz, E. Ahlswede, M. Walther, J. Wagner, and P. Koidl, "High performance InAs/Ga1-xInxSb superlattice infrared photodiodes," *Appl. Phys. Lett.*, vol. 71, p. 3251, 1997.

[6] K.W. Berryman, S.A. Lyon, and M. Segev, "Mid-infrared photoconductivity in InAs quantum dots," *Appl. Phys. Lett.,* vol. 70, p. 1861, 1997.

[7] J. Phillips, K. Kamath, and P. Bhattacharya, "Far-infrared photoconductivity in self organized InAs quantum dots," *Appl. Phys. Lett.*, vol. 72, p. 2020, 1998.

[8] D. Pan, E. Towe, and S. Kennerly, "Normal incidence intersubband (In,Ga)As/GaAs quantum dot infrared photodetectors," *Appl. Phys. Lett.*, vol. 73, p. 1937, 1998.

[9] Z. Chen, O. Baklenov, E.T. Kim, I. Mukhametzhanov, J. Tie, A. Madhukar, Z. Ye, and J.C. Campbell, "Normal incidence InAs/$Al_xGa_{1-x}As$ quantum dot infrared photodetectors with undoped active region," *J. Appl. Phys.*, vol. 89, p. 4558, 2001.

[10] I.N. Stranski and L. Krastanow, *Sitzungsberichte d. Akad. D. Wissenschaften in Wien*, Abt. IIb, Band 146, p.146, 1937.

[11] D. Leonard, M. Krishnamurthy, C.M. Reaves, S.P. Denbaars, and P.M. Petroff, "Direct formation of quantum-sized dots from uniform coherent islands of InGaAs on GaAs surfaces," *Appl. Phys. Lett.,* vol. 63, p. 3202, 1993.

[12] Q. Xie, P. Chen, A. Kalburge, T.R. Ramachandran, A. Nayfonov, A. Konkar, and A. Madhukar, "Realization of optically active strained InAs island quantum boxes on GaAs (100) via molecular beam epitaxy and the role of island induced strain fields," *J. Cryst. Growth,* vol. 150, p. 357, 1995.

[13] M. Tabuchi, S. Noda, and A. Sasaki, "Strain energy and critical thickness of heteroepitaxial InGaAs layers on GaAs substrate," *J. Cryst. Growth,* vol. 115, p. 169, 1991.

[14] P.R. Berger, K. Chang, P. Bhattacharya, J. Singh, and K.K. Bajaj, "Role of strain and growth conditions on the growth front profile of InxGa1-xAs on GaAs during the pseudomorphic growth regime," *Appl. Phys. Lett.,* vol. 53, p. 684, 1988.

[15] F.E. Prins, G. Lehr, M. Burkad, S. Nikitin, H. Schweizer, and G. Smith, "Quantum dots and quantum wires with high optical quality by implantation-induced intermixing," *Jpn. J. Appl. Phys.*, vol. 32, p. 6228, 1993.

[16] H. Jiang and J. Singh, "Strain distribution and electronic spectra of InAs/GaAs self-assembled dots: An eight-band study," *Phys. Rev. B*, vol. 56, p. 4696, 1996.

[17] R.M. Martin, "Elastic properties of ZnS structure semiconductors," *Phys. Rev. B.*, vol. 1, p. 4005, 1970.

[18] P.N. Keating, "Effect of invariance requirements on the elastic strain energy of crystals with application to the diamond structures," *Phys. Rev.*, vol. 145, p. 637, 1966.

[19] Y. Toda and Y. Arakawa, "Near-field spectroscopy of a single InGaAs self-assembled quantum dot," *IEEE J. Select. Topics Quantum Electron.,* vol. 6, p. 528, May-June 2000.

[20] D.L. Huffaker and D.G. Deppe, "Electroluminescence efficiency of 1.3 µm wavelength InGaAs/GaAs quantum dots," *Appl. Phys. Lett.*, vol. 73, p. 520, 1998.

[21] P. Bhattacharya, K. Kamath, J. Singh, D. Klotzkin, J. Phillips, H. Jiang, N. Chevela, T. Norris, T. Sosnowski, J. Laskar, and M. Ramanamurty, "In(Ga)As/GaAs self organized quantum dot laser: DC and small signal modulation properties," *IEEE Trans. Electron. Devices*, vol. 46, p. 871, May 1999.

[22] I. Vurgaftman and J. Singh, "Effect of spectral broadening and electron-hole scattering on carrier relaxation in GaAs quantum dots," *Appl. Phys. Lett.*, vol. 64, p. 232, 1994.

[23] B. Ohnesorge, M. Albrecht, J. Oshinowo, A. Forchel, and Y. Arakawa, "Rapid carrier relaxation in self-assembled InxGa1-xAs/GaAs quantum dots," *Phys. Rev. B*, vol. 54, p. 11532, 1996.

[24] T. Sosnowski, T. Norris, H. Jiang, J. Singh, K. Kamath, and P. Bhattacharya, "Rapid carrier relaxation in In0.4Ga0.6As/GaAs quantum dots characterized by differential transmission spectroscopy," *Phys. Rev. B-Condensed Matter*, vol. 57, p. R9423, 1998.

[25] J. Urayama, T.B. Norris, J. Singh, and P. Bhattacharya, "Observation of phonon bottleneck in quantum dot electronic relaxation," *Phys. Rev. Lett*, vol. 86, p. 4930, 2001.

[26] D. Klotzkin and P. Bhattacharya, "Temperature dependence of dynamic and dc characteristics of quantum dot and quantum well lasers: A comparative study," *J. Lightwave Technol.*, vol. 17, p. 1634, Sept. 1999.

[27] K. Mukai, N. Ohtsuka, H. Shoji, and M. Sugawara, "Emission from discrete levels in self-formed InGaAs/GaAs quantum dots by electric carrier injection: Influence of phonon bottleneck," *Appl. Phys. Lett.*, vol. 68, 3013, 1996.

[28] J. Phillips, P. Bhattacharya, S.W. Kennerly, D.W. Beekman, and M. Dutta, "Self-assembled InAs-GaAs quantum dot intersubband detectors," *IEEE J. Quant. Electron.*, vol. 35, p. 936, June 1999.

[29] Z. Ye, J.C. Campbell, Z. Chen, E.T. Kim, I. Mukhametzhanov, J. Tie, and A. Madhukar, "Bias-dependent dual-spectral InAs/$In_{0.15}Ga_{0.85}As$ quantum dot infrared photodetectors," in *Proc. IEEE LEOS Annual Meeting*, San Diego, CA, Nov. 2001, p. 766.

[30] A.D. Stiff, S. Krishna, P. Bhattacharya, and S. Kennerly, "Normal-incidence, high-temperature, mid-infrared, InAs/GaAs vertical quantum-dot infrared photodetector," *IEEE J. Quant. Electron.*, vol. 37, p. 1272, Nov. 2001.

[31] S.D. Gunapala and K.M.S.V. Bandara, *Homojunction and Quantum-Well Infrared Detectors*, M.H. Francombe and J.L. Vossen, Eds. San Diego, CA: Academic, 1995, p. 113-237.

[32] A.D. Stiff, S. Krishna, P. Bhattacharya, and S. Kennerly, "High-detectivity, normal-incidence, mid-infrared (~4 µm) InAs/GaAs quantum-dot detector operating at 150 K," *Appl. Phys. Lett.*, vol. 79, p. 421, 2001.

[33] H.C. Liu, "Noise gain and operating temperature of quantum well infrared photodetectors," *Appl. Phys. Lett.*, vol. 61, p. 2703, 1992.

[34] W.A. Beck, "Photoconductive gain and generation-recombination noise in multiple-quantum-well-infrared detectors," *Appl. Phys. Lett.*, vol. 63, p. 3589, 1993.

[35] S-W. Lee, K. Hirakawa, and Y. Shimada, "Bound-to-continuum intersubband photoconductivity of self-assembled InAs quantum dots in modulation-doped heterostructures," *Appl. Phys. Lett.*, vol. 75, p. 1428, 1999.

[36] J-W. Kim, J-E. Oh, S-C. Hong, C-H. Park, and T-K. Yoo, "Room temperature far infrared (8-10 mm) photodetectors using self-assembled InAs quantum dots with high detectivity," *IEEE Electron. Dev. Lett.*, vol. 21, p. 329, July 2000.

[37] M.A. Kinch, "Fundamental physics of infrared detector materials," *J. Electron. Mater.*, vol. 29, p. 809, 2000.

[38] J. Phillips, "Evaluation of the fundamental properties of quantum dot infrared detectors," *J. Appl. Phys.*, submitted for publication.